Published in final edited form as:
Synapse. 2011 December ; 65(12): 1309–1318. doi:10.1002/syn.20965.

Specific α4β2 Nicotinic Acetylcholine Receptor Binding of [F-18]Nifene in the Rhesus Monkey

A.T. Hillmer, **D.W. Wooten**, **J. Moirano**, **M. Slesarev**, **T.E. Barnhart**, **J.W. Engle**, **R.J. Nickles**, **D. Murali**, **M. Schneider**, **J. Mukherjee**[*], and **B.T. Christian**
Departments of Medical Physics, Psychiatry, Harlow Primate Center, Waisman Laboratory for Brain Imaging and Behavior, University of Wisconsin-Madison, Madison, Wisconsin

[*]Department of Psychiatry and Human Behavior, University of California, Irvine, California

Abstract

Objective—[F-18]Nifene is a PET radioligand developed to image α4β2* nicotinic acetylcholine receptors (nAChR) in the brain. This work assesses the *in vivo* binding and imaging characteristics of [F-18]nifene in rhesus monkeys for the development of PET experiments examining nAChR binding.

Methods—Dynamic PET imaging experiments with [F-18]nifene were acquired in 4 anesthetized macaca mulatta (rhesus) monkeys using a microPET P4 scanner. Data acquisition was initiated with a bolus injection of 109 ± 17 MBq [F-18]nifene and the time course of the radioligand in the brain was measured for up to 120 minutes. For two experiments, a displacement dose of (−)nicotine (0.03 mg/kg, i.v.) was given 45–60 minutes post injection and followed 30 minutes later with a second [F-18]nifene injection to measure radioligand nondisplaceable uptake. Time activity curves were extracted in the regions of the antereoventral thalamus (AVT), lateral geniculate nucleus region (LGN), frontal cortex, and the cerebellum (CB).

Results—The highest levels of [F-18]nifene uptake were observed in the AVT and LGN. Target-to-CB ratios reached maximum values of 3.3 ± 0.4 in the AVT and 3.2 ± 0.3 in the LG 30–45 minutes post-injection. Significant binding of [F-18]nifene was observed in the subiculum, insula cortex, temporal cortex, cingulate gyrus, frontal cortex, striatum, and midbrain areas. The (−)nicotine displaced bound [F-18]nifene to near background levels within 15 minutes post-drug injection. No discernable displacement was observed in the CB, suggesting its potential as a reference region. Logan graphical estimates using the CB as a reference region yielded binding potentials (BP_{ND}) of 1.6 ± 0.1 in the AVT, and 1.3 ± 0.1 in the LGN. The post-nicotine injection displayed uniform nondisplaceable uptake of [F-18]nifene throughout gray and white brain matter.

Conclusions—[F-18]Nifene exhibits rapid equilibration and a moderately high target to background binding profile in the α4β2* nAChR rich regions of the brain, thus providing favorable imaging characteristics as a PET radiotracer for nAChR assay.

Keywords

nicotinic acetylcholine receptors; PET; nifene

Corresponding Author: Waisman Center, University of Wisconsin-Madison, 1500 Highland Avenue, Madison, WI, 53593.

Introduction

Nicotinic acetylcholine receptors (nAChR) are pentameric ligand-gated ion channels present throughout the nervous system. These receptors play an important role in cognitive related functions including memory, attention, and mood (Perry et al. 1999), and help modulate neurochemical transmission (Sharples et al., 2000; Hogg et al., 2003). The α4β2 heteromeric subtype is the most plentiful nAChR subtype in the central nervous system, with greatest concentrations in the thalamus and a significant presence in the striatum and cortical regions (Han et al., 2003). Because α4 and β2 subunits exist in combinations other than exclusively α4β2, the notation α4β2* denotes predominantly α4β2 receptors but acknowledges potential binding to alternative receptor subtype combinations containing the α4 and β2 subunits. Clinically, α4β2 nAChRs are implicated in Alzheimer's disease, Parkinson's disease, schizophrenia, epilepsy, and substance abuse (Leonard et al., 2000; Paterson and Nordberg, 2000; Sihver et al., 2000; Hogg et al., 2003; Gotti and Clementi, 2004; Sacco et al., 2004).

Radioligands have been designed to image α4β2* nAChRs *in vivo* using positron emission tomography (PET) (for a recent review see Horti et al., 2010). PET studies examining α4β2* nAChRs in humans have been primarily limited to the radioligand 2-[F-18]-fluoro-A-85380 (2-[F-18]FA) (Valette et al., 1999; Mitkovski et al., 2005; Kimes et al., 2008). Studies using 2-[F-18]FA have examined changes in α4β2* nAChR binding due to aging (Ellis et al., 2009), Alzheimer's disease (Sabri et al., 2008), Parkinson's disease (Meyer et al., 2009), and epilepsy (Picard et al., 2006). Additional applications include characterization of nicotine occupancy and behavior of α4β2* nAChR binding in response to smoking (Brody et al., 2006; Mukhin et al. 2008). 2-[F-18]FA is hindered, however, by relatively slow *in vivo* kinetic behavior of the radiotracer, requiring imaging assay in excess of five hours (Chefer et al., 2003). Current advancement of α4β2* nAChR radioligand research is focused on developing compounds with more favorable *in vivo* behavior to shorten the period of data acquisition.

2-[F-18]-3-[2-((S)-3-pyrrolinyl)methoxy]pyridine, ([F-18]nifene), was designed as a moderate affinity analog of 2-[F-18]FA with the goal of yielding faster *in vivo* equilibration as a tradeoff for reduced α4β2* nAChR binding affinity (Pichika et al., 2006). This was accomplished by substituting the azetidine ring for the 3,4-dehydropyrrolidine ring found in 2-[F-18]FA (Figure 1). Pichika and colleagues reported on a preliminary study in the nonhuman primate, indicating that [F-18]nifene equilibrates rapidly in 30–40 minutes with sufficient target to background signal for *in vivo* assay of α4β2* nAChR binding. Using *in vitro* assay, they also reported a displacement of more than 95% bound [F-18]nifene by 300μM nicotine in rat brain homogenate.

The goal of this work is to provide additional *in vivo* characterization of [F-18]nifene in the rhesus monkey using a high resolution PET animal scanner in preparation for extending its use into disease specific animal models and ultimately into humans. Specifically, we report regional distribution of [F-18]nifene binding throughout the brain, its behavior in the blood, and the suitability of reference region methods of analysis.

Methods

1. Radiosynthesis

The radiosynthesis of [F-18]nifene follows the method previously described (Pichika et al., 2006). In summary, [F-18]fluoride was produced by irradiating [O-18]water on a 16 MeV GE PETtrace cyclotron and separated from the enriched water with a QMA cartridge (Waters). Using a customized chemistry processing control unit, [F-18]flouride was

azeotropically distilled with additions of anhydrous acetonitrile. The nitro precursor (1–2 mg), 2-nitro-3-[2((S)-*N*-*tert*-butoxycarbonyl-3-pyrroline)methoxy]pyridine (ABX, Raderberg, Germany) was dissolved in 250 μL anhydrous acetonitrile and 150 μL anhydrous dimethylsulfoxide and added to the dry [F-18]flouride. The mixture was then heated to 120° C for 18 minutes. The products were extracted with 6 mL methylene chloride and passed through a neutral alumina sep-pak. After removal of the methylene chloride the mixture was purified with a reverse phase HPLC C18 Prodigy 10 μm 250×10 mm column (Phenomenex) and a mobile phase of 60:40 acetonitrile:water with 0.1% triethylamine at 2.5 mL/min, with a UV detector attuned to 254 nm. The *N*-Boc-[F-18]nifene eluted at approximately 20 minutes and was subsequently dried by rotory evaporation. Volumes of 1 mL methylene chloride and 200 μL trifluoracetic acid were added to the dried intermediate and the mixture was then heated for 20 minutes at 80° C for deprotection. The product was then dried and pH adjusted to 7.0 with 10% sodium bicarbonate. To remove protected precursor, a second HPLC purification was performed under identical conditions as above with a flow rate of 1.5 mL/min. The [F-18]nifene product was eluted at approximately 9 minutes, dried of HPLC solvents, diluted in 10 mL saline, and passed through a 0.22 μm millipore filter for final formulation. Final product was analyzed by HPLC with a Nova-Pak C18 4 μm 3.9×300 mm column (Waters) and a mobile phase of 50:50 water:methanol with 0.1% triethylamine. [F-18]Nifene retention time was 7 minutes. The radiosynthesis required 2.5 hours resulting in estimated end of synthesis specific activities of 20–60 GBq/μmol, with total yields of 430–1200 MBq.

2. Animal Subjects

Four (3 male, 1 female; 9.0 ± 2.5kg) *macaca mulatta* (rhesus) subjects received [F-18]nifene PET scans. All housing and experimental procedures followed institutional guidelines and were approved by the Institutional Animal Care and Use Committee at the University of Wisconsin-Madison. For PET procedures, the subjects were first anesthetized with ketamine (10 mg/kg IM) and maintained on 1% - 1.5% isoflurane throughout the experiment. Atropine sulfate (0.27 mg IM) was given during experiments to minimize secretions. The radiotracer was administered as a 30 second bolus through a catheter placed in the saphenous vein. For MRI procedures subjects were first anesthetized with ketamine (10 mg/kg IM) and given 0.015 mg/kg dexmedetomidine immediately prior to the scan. Atipamazole (0.15 mg/kg) was administered immediately following procedure completion. Body temperature, breathing rate, heart rate, and SpO_2 levels were monitored and recorded for the duration of all experimental procedures. Following each experiment, the subject was returned to its cage and closely monitored until fully alert.

3. PET Data Acquisition

PET data were acquired using a Concorde microPET P4 scanner, with 7.8 cm and 19 cm in the axial and transaxial fields of view, respectively, and an intrinsic in-plane spatial resolution of 1.75 mm (Tai et al., 2001). Prior to data acquisition, the subject's head was placed in a sterotaxic headholder to reduce motion and provide similar image orientation across subjects. A transmission scan was then acquired for 518 seconds with a Co-57 rod source. Scan data acquisition was timed to start simultaneously with a bolus injection of 109 ± 17 MBq (2.9 ± 0.5 mCi) of [F-18]nifene. A minimum of 45 minutes of baseline [F-18]nifene data were acquired for all subjects and scans were 90–120 minutes in duration. The nicotine displacement dose was administered at earlier times once fast equilibration times were confirmed from the initial studies. The protocols for each of the studies are outlined in Table I. For the drug displacement studies, 0.03 mg/kg (−)nicotine was administered as a tartrate salt with the concentration calculated as mass of free base (Matta et al., 2007).

For two experiments arterial blood samples were acquired throughout the duration of the study, with rapid sampling immediately post-injection and slowing to 10 minute sampling intervals by the end of the study. Whole blood samples were acquired in volumes of 0.5 mL, mixed with 0.05 mL heparin, and assayed for radioactivity using a 2" NaI(Tl) well counter. Samples were then centrifuged for 5 minutes. Plasma volumes of 250 μL were withdrawn, mixed with 50 μL sodium bicarbonate and assayed for radioactivity. Ethyl acetate (EtAc) was used to denaturize the plasma proteins, and was then extracted for further radioactivity assay. The EtAc samples were concentrated and spotted on aluminum backed silica gel thin layer chromatography (TLC) plates (Whatman, Maidstone, Kent, England) in a mobile phase of 50:50 methanol:0.1M ammonium acetate. A phosphor plate was exposed overnight to the developed TLC plates, then read and analyzed with a Cyclone storage phosphor system (PerkinElmer) to detect the presence of radiolabeled components in the plasma samples.

4. MRI Data Acquisition and Coregistration

To provide anatomic localization of [F-18]nifene binding, an MRI scan was acquired for a single subject using a 3.0 T x750 GE Discovery scanner. Fast IR-prepared 3D gradient echo with high resolution sequencing was used to acquire T1 weighted images. Resulting images had matrix sizes of 256×256×124 corresponding to voxel dimensions of 0.55×0.55×0.80 mm^3. An early time frame integrated PET image from the same subject was coregistered to the T1- weighted MRI image. The Linear Image Registration Tool from the FMRIB Software Library (Jenkison et al., 2002) was utilized to calculate a rigid body transformation matrix aligning the individual subject's PET image to the subject's T1-weighted MRI image.

5. Data Analysis

List mode PET data were histogrammed into 2 minute time bins. The resulting sinograms were rebinned and reconstructed with 2-dimensional filtered backprojection using a 0.5 cm^{-1} ramp filter. Arc correction, scatter correction, attenuation correction, and scanner normalization were applied during reconstruction. Reconstructed images had a matrix size of 128×128×63 corresponding to voxel dimensions of 1.90×1.90×1.21 mm^3. A denoising algorithm was applied to the reconstructed images to improve the performance of voxel-based analysis (Christian et al., 2010). Circular regions of interest 2–3 voxels in diameter were drawn based on late summed images (25–45 minutes) to extract time-activity data in the brain regions of antereoventral region of the thalamus (AVT), region of the lateral geniculate nucleus (LGN), frontal cortex, striatum, subiculum, and midbrain. The distinction between LGN and AVT provides for convenient gross anatomical differentiation to more precisely describe activity distribution within the large structure of the thalamus. PET images were used for ROI selection based upon patterns of regional radiotracer distribution to maintain consistency across subjects since only one subject had a corresponding MRI image.

Potential specific binding in the cerebellum was examined by comparing the radiotracer time course before and after (−)nicotine injection. *In vitro* studies have found only small amounts of nicotine and α-bungarotoxin binding in the nonhuman primate cerebellum (Cimino et. al., 1992), as well as relatively low 5-[I-125]IA-85380 cerebellar binding *in vitro* (Kulak et. al., 2002), which has been supported by findings of the cerebellum as an appropriate reference region for 2-[F-18]FA (Chefer et. al., 2003). Logan graphical analysis (Logan et al., 1996) was performed with decay-corrected data and using the cerebellum as a reference region for nondisplaceable (ND) uptake to provide an estimate of distribution volume ratios (DVR). For the data presented here, the mean efflux term (i.e. $\overline{k_2}$) was not included in the DVR estimation, since target/cerebellum values become constant relatively quickly and the corresponding Logan plots rapidly become linear. Binding potentials

(BP_{ND}) were estimated from the DVR using the relationship BP_{ND} = DVR-1 (Innis et. al., 2007). Voxel-based parametric images of BP_{ND} were generated with the Logan method to visualize [F-18]nifene binding throughout the entire brain.

Results

[F-18]Nifene in the brain

[F-18]Nifene demonstrated high uptake in areas of the brain associated with high α4β2* nAChR density, mainly the thalamus. Time activity curves averaged across all subjects are illustrated in Figure 2. Peak activity was observed first in the cerebellum at 2–4 minutes followed by rapid clearance. Maximal uptake was found in the AVT and occurred within 5–9 minutes post-injection to peak levels as high as 0.09 %ID/cc. High levels of [F-18]nifene uptake were also observed in the LGN. The frontal cortex, subiculum, striatum, and midbrain all demonstrated moderate levels of uptake.

Target-to-cerebellum ratios are shown in Figure 3 for the AVT, LGN, and frontal cortex, providing an indication of the attainment of tracer pseudoequilibrium when the plots reach a plateau. AVT-to-cerebellum ratios peaked at an average of 36 minutes with a range of 29–45 minutes. Peak target-to-cerebellum values for each subject in the AVT, LGN, and frontal cortex are shown in Table II, revealing similar characteristics for the LGN and AVT regions. Regions of the frontal cortex had less variable ratios at reduced peak values.

[F-18]Nifene in the blood

The time course of [F-18]nifene in arterial plasma is shown in Figure 4. Estimated [F-18]nifene concentrations were obtained by adjusting the EtAc extracted fraction for EtAc/saline partitioning. TLC of this fraction showed no evidence of [F-18]nifene metabolites. We term this concentration the “uncorrected parent concentration” because full characterization of the metabolite profile was not determined. The estimated uncorrected parent fraction in the plasma was observed to decrease over time, starting around 50% immediately post injection, decreasing to approximately 30% at 15 minutes, and finally stabilizing between 30% and 20% for the remainder of the scan. Clearance rates in the uncorrected parent fraction from 20 - 60 minutes were calculated to be 0.015 min^{-1} and 0.020 min^{-1} for the studies with arterial sampling. At 40 minutes estimated cerebellum:uncorrected parent concentration ratios for these studies yielded values of 2.0 and 1.6.

(−)Nicotine displacement of [F-18]nifene

The injection of (−)nicotine caused rapid displacement of [F-18]nifene in all brain areas with specific binding (Fig. 5B–C). The time-activity curve of a (−)nicotine displacement experiment is shown in Figure 5A. Within 15 minutes post-(−)nicotine activity levels decreased to near cerebellar levels yielding AVT-to-cerebellum ratios of 1.3, 1.4, and 1.3 at this time. The introduction of a second injection of [F-18]nifene (post-(−)nicotine) exhibited rapid uptake, with activity time courses in the AVT and LGN similar in shape to that of the cerebellum. In blockade studies 30 minutes after the second [F-18]nifene injection, AVT-to-cerebellum ratios were 1.7 and 1.5, suggesting a slight reduction in the (−)nicotine blockage. Activity levels in the cerebellum appeared unaffected by the presence of (−)nicotine. Figure 6A displays the close agreement of the post-(−)nicotine data to the curve extrapolated from the pre-(−)nicotine data, revealing a constant washout rate of radiotracer. Figure 6B illustrates cerebellar time-activity curves of the different injections (pre- and post-(−)nicotine) from the same experiment with nearly identical concentrations.

Specific binding of [F-18]Nifene

Based upon the lack of observable (−)nicotine displacement of [F-18]nifene in the cerebellum, BP_{ND} was calculated in various regions of the brain using the cerebellum as a reference region. A Logan plot for various areas of [F-18]nifene binding (subject M4) is shown in Figure 7, and the regional BP_{ND} estimates for all the subjects are given in Table II.

A [F-18]nifene DVR parametric image was created for the subject with an accompanying MRI (subject M3) and is shown in Figure 8 to illustrate [F-18]nifene binding throughout the brain. These images were transformed into an atlas space developed in-house (based on Paxinos et. al., 2000.) with predefined regions of interest. The rank order of BP_{ND} values for regions with significant [F-18]nifene binding based upon regions where $BP_{ND} > 0.25$ are as follows: AVT: 1.50, LGN: 1.15, frontal cortex: 0.64, cingulate gyrus: 0.51, caudate: 0.44, putamen: 0.43, midbrain areas: 0.40, insular cortex: 0.38, subiculum: 0.33, somatosensory cortex: 0.33, parietal cortex: 0.33, prefrontal cortex: 0.32, anterior cingulate cortex: 0.29. All other subjects appeared to exhibit elevated binding in approximately these same regions.

Discussion

In vivo examination of the α4β2* nAChR using 2-[F-18]FA PET has provided valuable information to the scientific community in the field of tobacco addiction. These preliminary studies have provided a foundation for extending research concerning the involvement of α4β2* nAChR in neurodevelopment and neurodegenerative disease. Improvement in the imaging characteristics of α4β2* nAChR radiotracers will undoubtedly hasten the development of molecular imaging methods for *in vivo* assessment of this system. Preliminary studies of [F-18]nifene in animal models have demonstrated high *in vitro* α4β2* binding in rat brain slices which could be almost completely dissociated by (−)nicotine (Pichika et al. 2006), and *in vitro* binding sensitivity to acetylcholine competition (Easwaramoorthy et al. 2007). Encouraged by these results, our goal is to examine the imaging characteristics of [F-18]nifene in the nonhuman primate model using high resolution PET imaging.

Rapid uptake and specific binding of [F-18]nifene was observed throughout brain regions with known α4β2* expression. The highest levels of [F-18]nifene binding were observed in the AVT, with target-to-cerebellum ratios ranging from 2.6 to 3.8 and reaching a plateau at an average of 36 minutes. This is dramatically shorter than the time required for achieving this point of equilibration using 2-[F-18]FA (>7 hr) (Chefer et al. 2003) and translates into a shorter experimental procedure. Using high resolution PET imaging, we were able to evaluate [F-18]nifene binding in extrathalamic brain regions for comparison with autoradiography findings with [H-3]nicotine and [H-3]cytosine binding in the rhesus monkey (Han et. al., 2003). The autoradiography results reported high binding in the AVT and LGN regions, with moderate binding in the subiculum, midbrain areas, and various cortical areas, with lower binding in the striatum. Our observations generally agreed with these findings. There was, however, a significant lack of [F-18]nifene binding in non-auditory regions of temporal cortex compared to the findings of Han and colleagues (2003). Additionally, binding of [F-18]nifene in the striatum was found to be elevated compared to the autoradiography work.

In these experiments, arterial blood sampling was performed on two subjects. The analyses of these samples was restricted to assay of the EtAc extracted component and preliminary inspection of radiolabeled metabolites using TLC. The EtAc radiolabeled component consisted of only a single species of radiolabeled product, which was taken to be [F-18]nifene based upon the profile of the accompanying [F-18]nifene standard TLC run. A non-linear time-dependant reduction in radioactivity was found in the EtAc fraction

compared to the aqueous component, as the EtAc fraction fell to between 20% and 30% 60 minutes post-injection (Figure 4B). This suggests buildup of less lipophilic (not extracted by EtAc) radiolabeled species over the course of the experiment. A similar profile was reported for 2-[F-18]FA using HPLC methods to separate the distinct radiolabeled components (Chefer et al. 2003).

More rigorous analyses of [F-18]nifene plasma samples will be required to fully characterize the potential presence of radiolabeled metabolites that may confound interpretation of the radiolabeled signal in the brain tissue, perhaps using protein denaturization via acetonitrile instead of ethyl acetate. Nicotine is known to result in several metabolites that are further broken down (Hukkanen et al., 2005). One of the major pathways that nicotine follows is demethylation to provide nornicotine, which is an active metabolite. Some of the prolonged occupancy at the α4β2 receptors has been attributed to this nornicotine metabolite (Valette et al., 2003). [F-18]Nifene contains a secondary amine similar to that found in nornicotine, suggesting [F-18]nifene could be metabolized to nornicotine as well. Preliminary studies and brain metabolite analysis were carried out to examine the [F-18]nifene profile in the rat brain and revealed only the presence of the radiolabeled parent across the blood brain barrier (Easwaramoorthy et al. 2008).

The cerebellum was selected as a reference region in the brain to represent the behavior of [F-18]nifene in the absence of measurable α4β2* receptor specific binding. This choice was initially guided by previous studies in the rhesus monkey using 2-[F-18]FA which reported differences in cerebellar total distribution volume of only 3% when comparing baseline studies with cytisine blocking studies (1 mg/kg, s.c.) (Chefer et. al. 2003). Further, *in vitro* findings have reported very low levels of cerebellar α4β2* in the squirrel (Kulak et al., 2002) and cynomolgus monkeys (Cimino et al., 1992). This lack of specific α4β2* binding in the cerebellum is consistent with our post-(−)nicotine results (see Figure 6). Qualitatively, there was no observed perturbation in the cerebellar time course following the administration of (−)nicotine, which was evident in the other regions examined. These measurements do not discount the presence of specific cerebellar α4β2* binding to [F-18]nifene, as small, yet significant α4β2* expression has been reported in other nonhuman primates species (Villemagne et al., 1997) and humans (Marutle et. al., 1998; Kimes et. al., 2008). However, for [F-18]nifene it is probable that the PET imaging signal lacks the sensitivity to distinguish the presence of specific α4β2* binding from the dominant nondisplaceable component of the PET signal in the cerebellum, making it an acceptable reference region. The potential effects of receptor upregulation in this region, however, must be considered for research involving chronic nicotine administration as suggested by Le Foll et al. (2007).

The Logan graphical method was applied to the brain α4β2* target regions to obtain estimates of [F-18]nifene BP_{ND}. Even without the inclusion of the mean efflux term ($\overline{k_2}$) in the Logan equation, the data are shown to achieve a rapid equilibration period for linearization (Logan et al. 1996). Figure 7 illustrates that the period of linearization (steady state) was achieved within approximately 20 minutes in the thalamus. These studies suggest that the rapid equilibration of [F-18]nifene will produce stable estimates of BP_{ND} throughout the regions of the brain with data acquisition periods of 45 – 60 minutes.

When compared to 2-[F-18]FA (Chefer et. al., 2003), average [F-18]nifene BP_{ND} values for the four subjects were slightly lower in the thalamus (2.1 vs. 1.6) and similar in the extrathalamic regions. This serves only as a general comparison between compounds because BP_{ND} measures depend on the size and heterogeneity of the defined ROI (due to partial volume effects) as well as acquisition and preprocessing steps involved in the experiment. For example, reducing the size of the AVT ROI reported in Table III by half

increases the BP_{ND} by 20%, which is in close agreement with reported 2-[F-18]FA thalamus BP_{ND} values. An experimental design using the same subjects and the same acquisition and analysis schemes will be required to directly compare the imaging characteristics of 2-[F-18]FA and [F-18]nifene. Based upon the cerebellum-to-plasma ratios, however, we speculate that V_{ND} is lower for [F-18]nifene (~2) than for 2-[F-18]FA (~3.3) (Chefer et. al. 2003).

The rapid (−)nicotine displacement of [F-18]nifene from the tissue suggests the dissociation rate constant, k_{off}, is relatively high (i.e. fast). 2-[F-18]FA also demonstrates rapid dissociation following the introduction of (−)nicotine (LeFoll et. al. 2007). At this time, however, we cannot provide a comparison of k_{off} for the two radiotracers. Such a measurement will require carefully designed PET experiments to uncouple the dissociation process from tissue-to-plasma efflux constant, k_2, which may be the limiting process for radiotracer tissue clearance of these compounds (Gallezot et. al. 2008).

Conclusion

This study demonstrates favorable imaging characteristics of [F-18]nifene for *in vivo* α4β2* nAChR assay. The apparent lack of measurable specific binding in the cerebellum and elevated extrathalamic binding and rapid *in vivo* kinetics suggest [F-18]nifene is suitable for α4β2* nAChR research in the rhesus monkey. These data also promote the extension of [F-18]nifene use in human research, however, additional validation will be required to closely examine its characteristics in blood and potential reference region binding.

Acknowledgments

The authors thank the following for their contributions to this research: Dr. Alex Converse for contributions with the rhesus monkey atlas. Elizabeth Ahlers and Julie Larson for data acquisition and processing; the staff at the Harlow Center for Biological Psychology at the University of Wisconsin (RR000167) for nonhuman primate handling. This work was supported by NIH grants CA143188, AA017706.

References

Brody AL, Mandelkern MA, London ED, Olmstead RE, Farahi J, Scheibal BA, Jou J, Allen V, Tiongson E, Chefer S, Koren A, Mukhin AG. Cigarette smoking saturates brain α4β2 nicotinic acetylcholine receptors. Arch Gen Psychiat. 2006; 63:907–915. [PubMed: 16894067]

Chefer SI, London ED, Koren AO, Pavlova OA, Kurian V, Kimes AS, Horti AG, Mukhin AG. Graphical analysis of 2-[18-F]FA binding to nicotinic acetylcholine receptors in rhesus monkey brain. Synapse. 2003; 48:25–34. [PubMed: 12557269]

Chefer SI, Pavlova OA, Zhang Y, Vaupel DB, Kimes AS, Horti AG, Stein E, Mukhin AG. NIDA522131, a new radioligand for imaging extrathalamic nicotinic acetylcholine receptors: in vitro and in vivo evaluation. J Neurochem. 2008; 104:306–315. [PubMed: 17986233]

Christian BT, Vandehey NT, Floberg JM, Mistretta CA. Dynamic PET Denoising with HYPR Processing. J Nucl Med. 2010; 51:1147–1154. [PubMed: 20554743]

Cimino M, Marini P, Fornasari D, Cattabeni F, Clementi F. Distribution of nicotinic acetylcholine receptors in cynomolgus monkey brain and ganglia: localization of alpha 3 subunit mRNA, alpha-bungarotoxin and nicotine binding sites. Neuroscience. 1992; 51:77–86. [PubMed: 1465189]

Easwaramoorthy B, Pichika R, Collins D, Potkin SG, Leslie FM, Mukherjee J. Effect of Acetylcholinesterase Inhibitors on the Binding of Nicotinic a4b2 Receptor PET Radiotracer, 18 F-Nifene : A Measure of Acetylcholine Competition. Synapse. 2007; 36:29–36. [PubMed: 17068780]

Easwaramoorthy B, Pichika R, Constantinescu C, Saigal N, Coleman R, Mukherjee J. Measurement of brain and plasma metabolites of 18F-Nifene. J Nucl Med. 2008; 49:142P. [PubMed: 18077523]

Ellis JR, Nathan PJ, Villemagne VL, Mulligan RS, Ellis KA, Tochon-Danguy HJ, Chan JG, O'Keefe GJ, Bradley J, Savage G, Rowe CC. The relationship between nicotinic receptors and cognitive

functioning in healthy aging: An in vivo positron emission tomography (PET) study with 2-[^{18}F]Fluoro-A-85380. Synapse. 2009; 63:752–763. [PubMed: 19484724]

Gallezot J-D, Bottlaender MA, Delforge J, Valette H, Saba W, Dolle F, Coulon CM, Ottaviani MP, Hinnen F, Syrota A, Gregoire M-C. Quantification of cerebral nicotinic acetylcholine receptors by PET using 2-[18F]fluoro-A-85380 and the multiinjection approach. J Cereb Blood Flow Metab. 2008; 28:172–189. [PubMed: 17519978]

Gotti C, Clementi F. Neuronal nicotinic receptors: from structure to pathology. Prog Neurobiol. 2004; 74:363–396. [PubMed: 15649582]

Han ZY, Zoli M, Cardona A, Bourgeois JP, Changeux JP, Le Novère N. Localization of [^{3}H]nicotine, [^{3}H]cytisine, [^{3}H]epibatidine, and [^{125}I]α-bungarotoxin binding sites in the brain of Macaca mulatta. J Comp Neurol. 2003; 461:49–60. [PubMed: 12722104]

Hogg RC, Raggenbass M, Bertrand D. Nicotinic acetylcholine receptors: from structure to brain function. Rev Physiol Bioch P. 2003; 147:1–46.

Horti AG, Gao Y, Kuwabara H, Dannals RF. Development of radioligands with optimized imaging properties for quantification of nicotinic acetylcholine receptors by positron emission tomography. Life Sci. 2010; 86:575–584. [PubMed: 19303028]

Hukkanen J, Iii PJ, Benowitz NL. Metabolism and Disposition Kinetics of Nicotine. Pharmacology. 2005; 57:79–115.

Innis RB, Cunningham VJ, Delforge J, Fujita M, Gjedde A, Gunn RN, Holden J, Houle S, Huang S-C, Ichise M, Iida H, Ito H, Kimura Y, Koeppe RA, Knudsen GM, Knuuti J, Lammertsma AA, Maguire RP, Mintun MA, Morris ED, Parsey R, Price JC, Silfstein M, Sossi V, Suhara T, Votaw JR, Wong DF, Carson RE. Consensus nomenclature for *in vivo* imaging of reversibly binding radioligands. J Cereb Blood Flow Metab. 2007; 27:1533–1539. [PubMed: 17519979]

Jenkinson M, Bannister P, Brady M, Smith S. Improved Optimization for the Robust and Accurate Linear Registration and Motion Correction of Brain Images. NeuroImage. 2002; 17:825–841. [PubMed: 12377157]

Kimes AS, Chefer SI, Matochik JA, Contoreggi CS, Vaupel DB, Stein EA, Mukhin AG. Quantification of nicotinic acetylcholine receptors in the human brain with PET: bolus plus infusion administration of 2-[^{18}F]F-A85380. NeuroImage. 2008; 39:717–727. [PubMed: 17962044]

Kulak JM, Musachio JL, McIntosh M, Quik M. Declines in Different β2* Nicotinic Receptor Populations in Monkey Striatum after Nigrostriatal Damage. J Pharmacol Exp Ther. 2002; 303:633–639. [PubMed: 12388645]

Le Foll B, Chefer SI, Kimes AS, Shumway D, Goldberg SR, Stein EA, Mukhin AG. Validation of an extracerebral reference region approach for the quantification of brain nicotinic acetylcholine receptors in squirrel monkeys with PET and 2-^{18}F-Fluoro-A-85380. J Nucl Med. 2007; 48:1492–1500. [PubMed: 17704243]

Leonard S, Breese C, Adams C, Benhammou K, Gault J, Stevens K, Lee M, Adler L, Olincy A, Ross R, Freedman R. Smoking and schizophrenia: abnormal nicotinic receptor expression. Eur J Pharmacol. 2000; 393:237–242. [PubMed: 10771019]

Logan J, Fowler JS, Volkow D, Wang GJ, Ding YS, Alexoff DL. Distribution volume ratios without blood sampling from graphical analysis of PET data. J Cereb Blood Flow Metab. 1996; 16:834–840. [PubMed: 8784228]

Marutle A, Warpman U, Bodganovic N, Nordberg A. Regional distribution of subtypes of nicotinic receptors in human brain and effect of again studied by (±)-[^{3}H]epibatidine. Brain Research. 1998; 801:143–149. [PubMed: 9729344]

Matta SG, et al. Guidelines on nicotine dose selection for in vivo research. Psychopharmacology. 2007; 190:269–319. [PubMed: 16896961]

Meyer PM, Strecker K, Kendziorra K, Becker G, Hesse S, Woelpl D, Hensel A, Patt M, Sorger D, Wegner F, Lobsien D, Barthel H, Brust P, Gertz HJ, Sabri O, Schwarz J. Reduced α4β2*-nicotinic acetylcholine receptor binding and its relationship to mild cognitive and depressive symptoms in Parkinson disease. Arch Gen Psychiat. 2009; 66:866–877. [PubMed: 19652126]

Mitkovski S, Villemagne VL, Novakovic KE, O'Keefe G, Tochon-Danguy H, Mulligan RS, Dickinson KL, Saunder T, Gregoire MC, Bottlaender M, Dolle F, Rowe CC. Simplified quantification of

nicotinic receptors with 2[18F]F-A-85380 PET. Nucl Med Biol. 2005; 32:585–591. [PubMed: 16026705]

Mukhin AG, Kimes AS, Chefer SI, Matochik JA, Contoreggi CS, Horti AG, Vaupel DB, Pavlova O, Stein E. Greater nicotinic acetylcholine receptor density in smokers than in nonsmokers: a PET study with 2-18F-FA-85380. J Nucl Med. 2008; 49:1628–1635. [PubMed: 18794265]

Paterson D, Nordberg A. Neuronal nicotinic receptors in the human brain. Prog Neurobiol. 2000; 61:75–111. [PubMed: 10759066]

Paxinos, G.; Huang, XF.; Toga, AW. The rhesus monkey brain. New York: Academic Press; 2000.

Perry E, Walker M, Grace J, Perry R. Acetylcholine in mind: a neurotransmitter correlate of consciousness? Trends Neurosci. 1999; 22:273–280. [PubMed: 10354606]

Picard F, Bruel D, Servent D, Saba W, Fruchart-Gaillard C, Schollhorn-Peyronneau MA, Roumenov D, Brodtkorb E, Zuberi S, Gambardella A, Steinborn B, Hufnagel A, Valette H, Bottlaender M. Alteration of the in vivo nicotinic receptor density in ADNFLE patients: a PET study. Brain. 2006; 129:2047–2060. [PubMed: 16815873]

Pichika R, Easwaramoorthy B, Collins D, Christian BT, Shi B, Narayanan TK, Potkin SG, Mukherjee J. Nicotinic α4β2 receptor imaging agents: part II. Synthesis and biological evaluation of 2-[^{18}F]fluoro-3-[2-((S)-3-pyrrolinyl)methoxy]pyridine (^{18}F-nifene) in rodents and imaging by PET in nonhuman primate. Nucl Med Biol. 2006; 33:295–304. [PubMed: 16631077]

Quik M, Polonskaya Y, Gillespie A, Jakowec M, Lloyed GK, Langston JW. Localization of Nicotinic Receptor Subunit mRNAs in Monkey Brain by In Situ Hybridization. J Comp Neurol. 2000; 425:58–69. [PubMed: 10940942]

Sabri O, Kendziorra K, Wolf H, Gertz HJ, Brust P. Acetylcholine receptors in dementia and mild cognitive impairment. Eur J Nucl Med Mol I. 2008; 35:S30–S45.

Sacco KA, Bannon KL, George TP. Nicotinic receptor mechanisms and cognition in normal states and neuropsychiatric disorders. J Psychopharmacol. 2004; 18:457–474. [PubMed: 15582913]

Sharples CG, Kaiser S, Soliakov L, Marks MJ, Collins AC, Washburn M, Wright E, Spencer JA, Gallagher T, Whiteaker P, Wonnacott S. UB-165: a novel nicotinic agonist with subtype selectivity implicates the α4β2* subtype in the modulation of dopamine release from rat striatal synaptosomes. J Neurosci. 2000; 20:2783–2791. [PubMed: 10751429]

Sihver W, Nordberg A, Långström B, Mukhin AG, Koren AO, Kimes AS, London ED. Development of ligands for in vivo imaging of cerebral nicotinic receptors. Behav Brain Res. 2000; 113:143–157. [PubMed: 10942041]

Tai YC, Chatziioannou A, Siegel S, Young J, Newport D, Goble RN, Nutt RE, Cherry SR. Performance evaluation of the microPET P4: a PET system dedicated to animal imaging. Phys Med Biol. 2001; 46:1856–1862.

Valette H, Bottlaender M, Dollé F, Guenther I, Fuseau C, Coulon C, Ottaviani M, Crouzel C. Imaging central nicotinic acetylcholine receptors in baboons with [^{18}F]Fluoro-A-85380. J Nucl Med. 1999; 40:1374–1380. [PubMed: 10450691]

Valette H, Bottlaender M, Dollé F, Coulon C, Ottaviani, Syrota A. Long-lasting occupancy of central nicotinic acetylcholine receptors after smoking: a PET study in monkeys. J Neurochem. 2003; 84:105–111. [PubMed: 12485406]

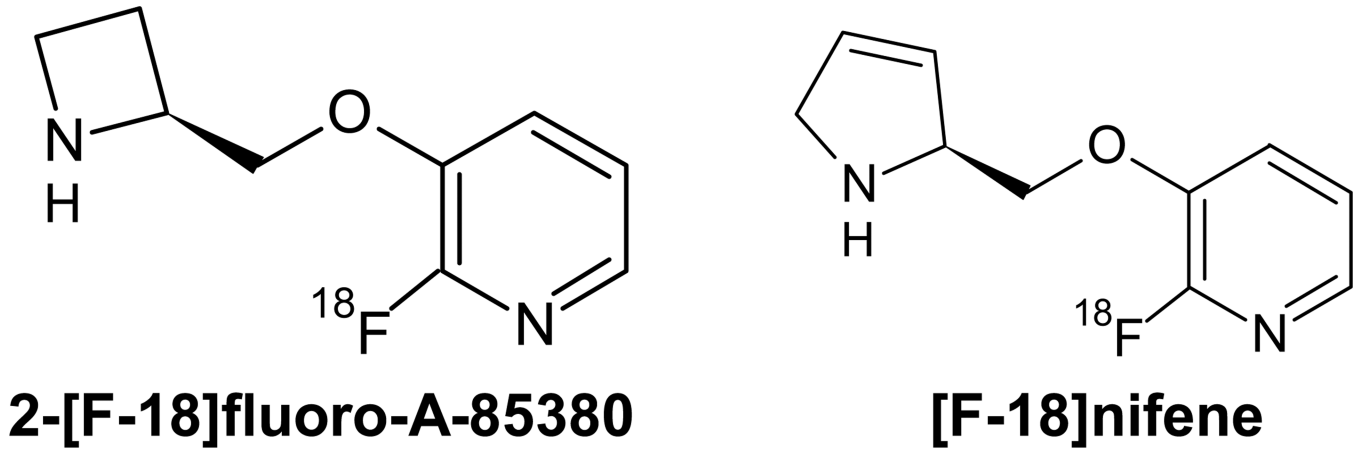

Fig. 1.
Chemical structures for the α4β2 specific nAChR radioligands 2-[F-18]fluoro-A-85380 (left) and [F-18]nifene (right).

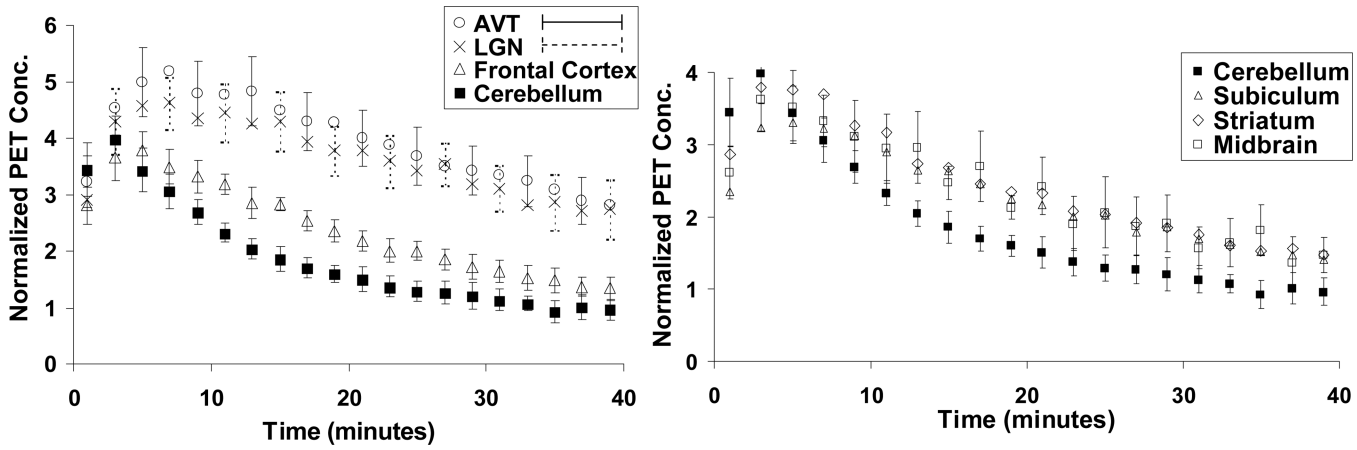

Fig. 2.

Averaged time-activity curves of [F-18]nifene binding in high receptor density (left) and low receptor density (right) regions of the rhesus monkey brain. Values are normalized to injected activity and multiplied by subject weight (kBq/cc/i.d.×kg ×1000). Note the slightly different scales on the y-axes. To enhance visual clarity, error bars of alternating points were shown for the LGN and AVT, and error bars for only the midbrain were shown for low receptor density regions, as errors were similar across regions for the striatum, subiculum, and midbrain.

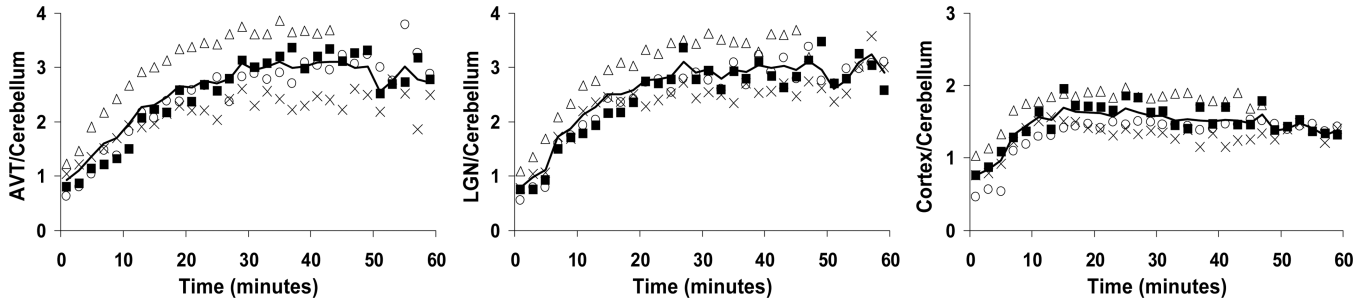

Fig. 3.

Target-to-cerebellum ratios in the AVT (left), LGN (center), and frontal cortex (right). Each distinct symbol represents a different study reported here. The dark line shows the average ratio of the four studies, with only 3 studies averaged for times after 45 minutes.

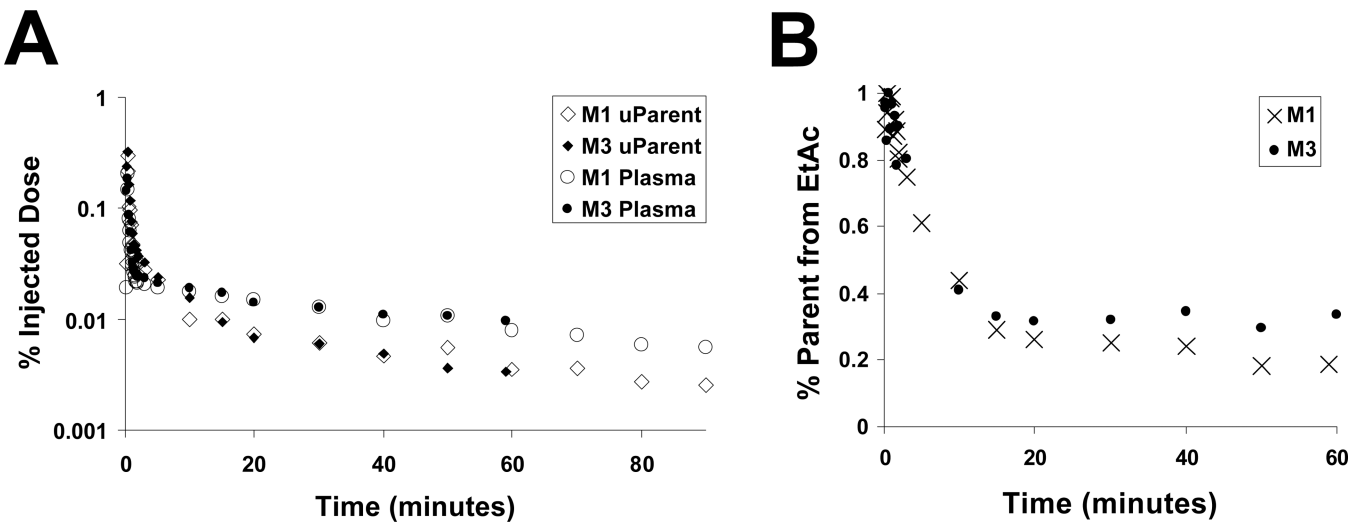

Fig. 4.

Behavior of [F-18]nifene in the blood. (**A**) Arterial plasma time-activity curves of [F-18]nifene. The data shown represent the activity measured in the plasma (♦) and uncorrected parent (●) relative to the injected dose. (**B**) Percentage of total activity in the plasma estimated in the parent fraction.

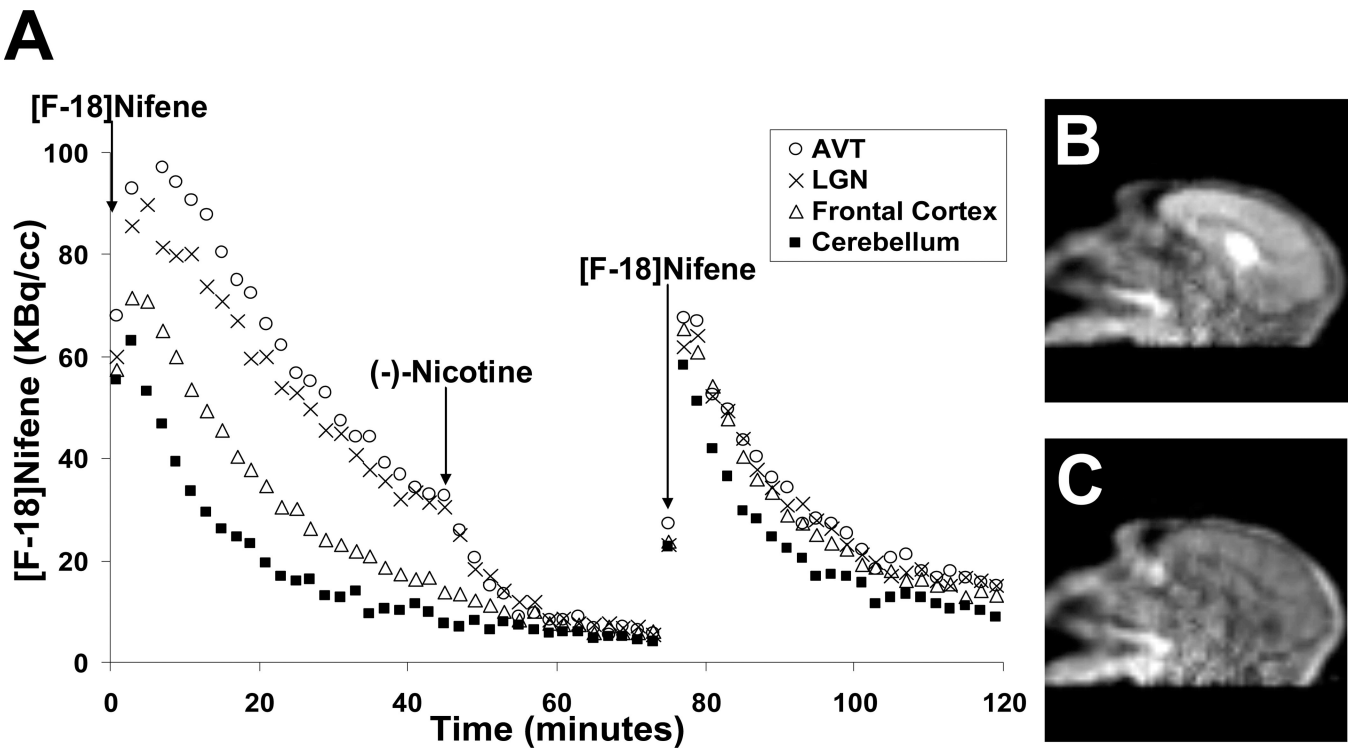

Fig. 5.

(**A**) Time-activity curves (uncorrected for radioactive decay) of [F-18]nifene in the AVT and LGN regions, frontal cortex, and cerebellum over the course of a single 120 minute scan (M3) with injections of (−)nicotine at 45 minutes and 79 MBq [F-18]nifene at 75 minutes (denoted by arrows). (**B**) and (**C**) on the right show summed frames from 20–30 minutes and 60–70 minutes, respectively.

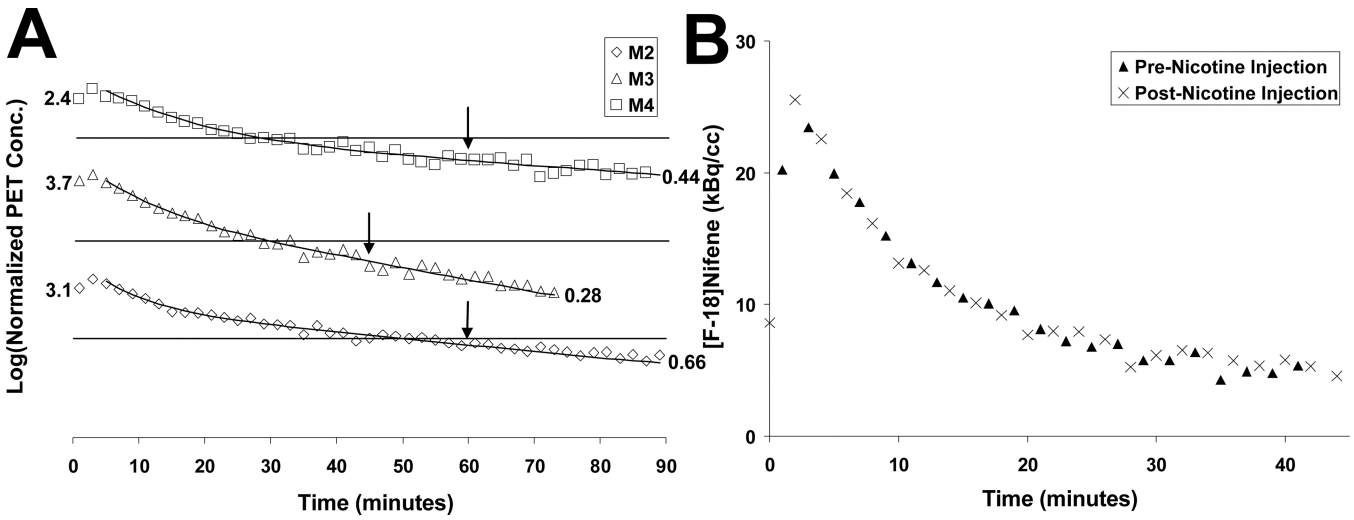

Figure 6.

Cerebellum Time Activity Curves. (**A**) The cerebellar time course for the three displacement studies. Discrete data points denote observed data. Solid curves were the result of fitting a bi-exponential function to the data up until time of (−)nicotine challenge; the line after the arrow illustrates values extrapolated from the time course of the pre-nicotine data. The arrows denote the time of (−)nicotine injection. Scale on the y-axis is indicated by the numbers representing the first and last data point. Lines represent normalized PET concentrations of 1. (**B**) PET concentrations from the same experiment (M4) in the cerebellum from the initial pre-nicotine injection(▲) and cerebellum concentrations from the post-nicotine blockade injection(×). Values are normalized to injected activity.

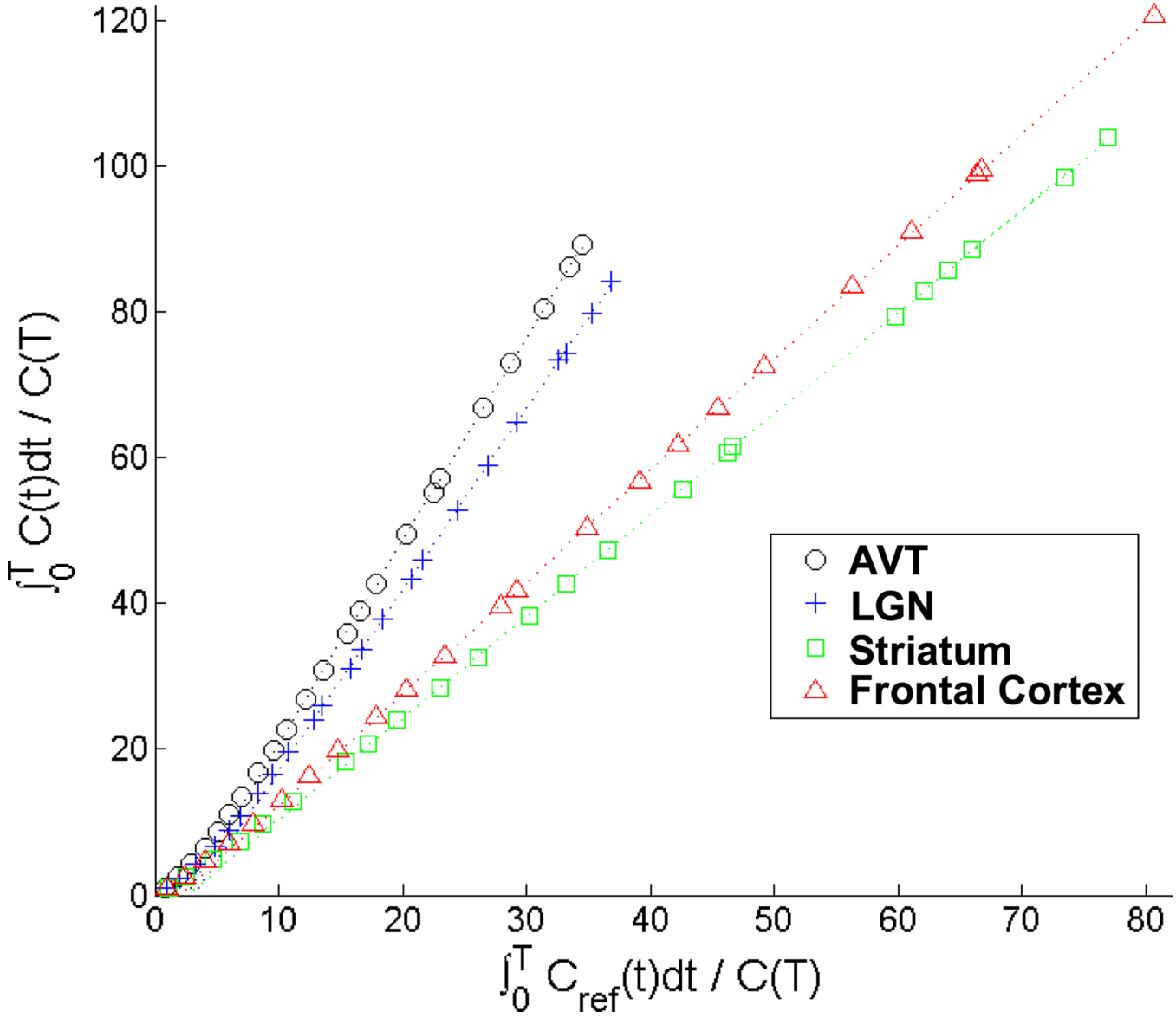

Fig. 7.

Logan plot of various regions of interest for a [F-18]nifene study (M4). The lines shown are fit to the data following the period of linearization (t*), which was determined to occur at 20 minutes scan time.

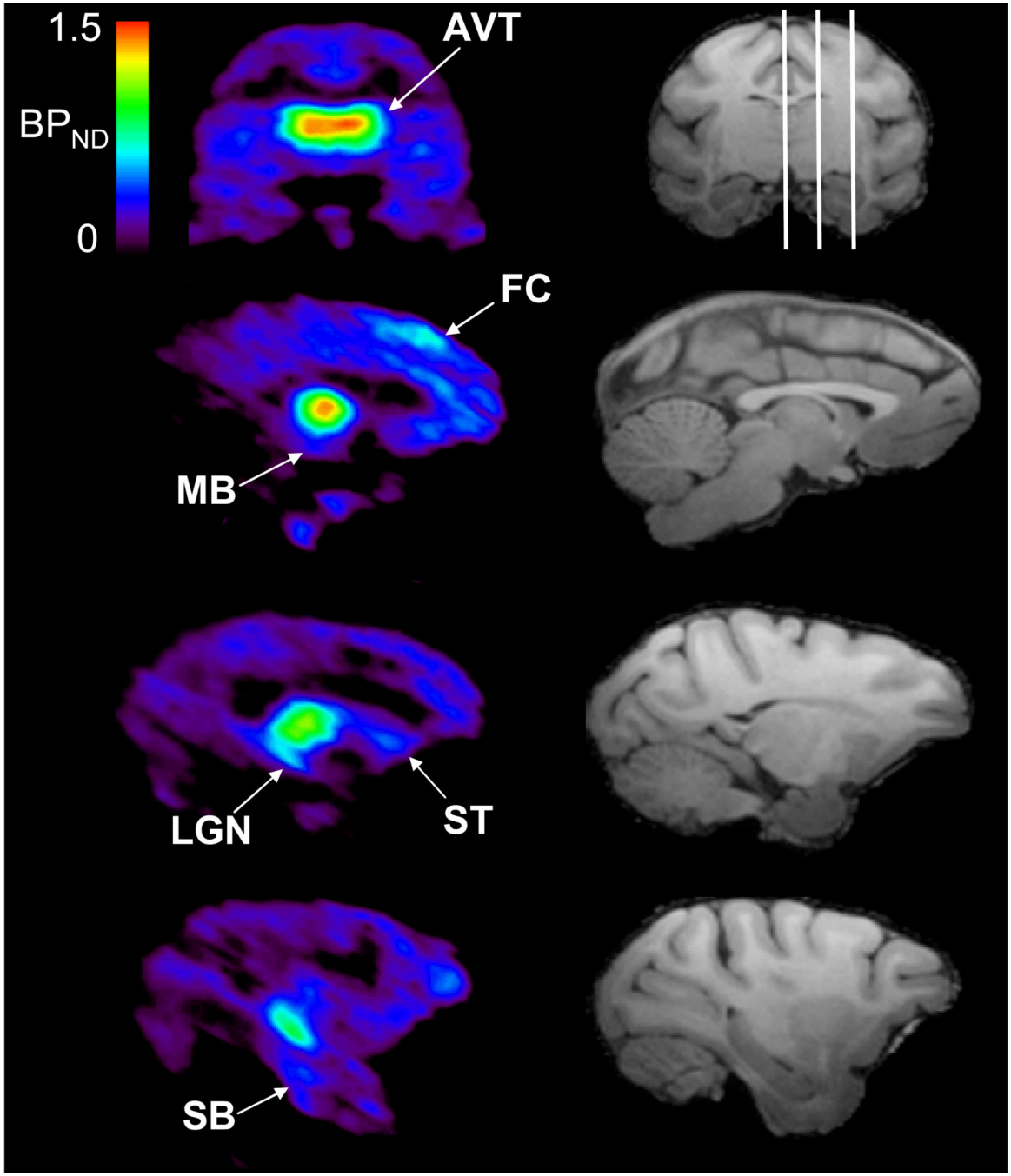

Fig. 8.

Specific binding of [F-18]nifene in the rhesus monkey. The left column is voxel-wise BP_{ND} images of [F-18]nifene calculated with the Logan graphical method. The right column is a skull stripped T1 magnetic resonance image, with the white lines on the coronal slice delineating the planes of the three sagittal slices illustrated below. Regions of significant ($BP_{ND} > 0.25$) specific binding highlighted in the PET images include the following regions: AVT, superior frontal cortex (FC), midbrain (MB), striatum (ST), LGN, and subiculum (SB).

Table I

Summary of Experimental Protocols for Each Subject

Subject #	Subject Mass (kg)	Total Scan Time (min)	Time (min), 0.03 mg/kg Nicotine Injection*	Time (min), Second [F-18]Nifene Injection
M1	11.5	90	N/A	N/A
M2	9.0	90	60	N/A
M3	9.8	120	60	90
M4	6.7	120	45	75

* based upon (−)nicotine free base mass

Table II

Measured Maximum Target/Cerebellum Ratios

Subject	AVT	LGN	Frontal Cortex
M1	3.4	3.2	1.7
M2	2.6	2.7	1.5
M3	3.2	2.1	1.5
M4	3.8	3.6	1.9
mean ± s.d.	3.25 ± 0.43	3.15 ± 0.32	1.65 ± 0.17

Table III

Calculated BP_{ND} for Various Brain Regions

Subject	AVT	LGN	Striatum	Frontal Cortex	Midbrain	Subiculum
M1	1.43	1.20	0.25	0.24	0.17	0.53
M2	1.56	1.38	0.40	0.24	0.52	0.42
M3	1.50	1.14	0.38	0.40	0.40	0.33
M4	1.80	1.29	0.41	0.52	0.20	0.32
mean ± s.d.	1.57 ± 0.16	1.25 ± 0.10	0.36 ± 0.08	0.35 ± 0.14	0.35 ± 0.15	0.40 ± 0.10